Research Article Vol. 15, No. 1 / 1 Jan 2024 / Biomedical Optics Express 306
Biomedical Optics EXPRESS

Plasmon enhanced luminescence of Tb/Eu co-doped film by Au NRs-PVA nanocomposite film

Lianyu Zhang,[1] Jinhua Liu,[1] Linlin Tian,[1] Dong Zhang,[1,2] and Qingru Wang[1,*]

[1] *School of Physical Science and Information Technology, Shandong Provincial Key Laboratory of Optical Communication Science and Technology, Liaocheng University, Liaocheng 252059, China*
[2] *zhangdong@lcu.edu.cn*
[*] *wangqingru@lcu.edu.cn*

Abstract: Plasmonic nanostructures have great potential for improving the radiation properties of emitters. Here, the plasmonic Au nanorods-PVA nanocomposite films are used to uniformly improve the photoluminescence of Tb/Eu co-doped PMMA film within the local micro-region. Under the excitation of 292 nm, the maximum enhancement factor is 37.2-fold for emission at 612 nm and 21.6-fold for emission at 545 nm. Moreover, the finite different time domain simulations are developed to further explain the experimental results. It is indicated that the modulation of luminescence can be attributed to the increase of the local density of optical states through the Purcell effect and the improvement of the energy transfer efficiency between Tb and Eu. Under the excitation of 360 nm, the maximum enhancement factor is about 71.5-fold. In this case, the Au nanorods are mainly used for modulating the emission process at 612 nm, which deduced a greater enhancement factor at 612 nm. This study provides a deep understanding of the interactions between rare earth ions co-doped materials and plasmonic nanostructures, building a bridge to fabricate a useful platform for several applications, such as thin film-based detectors and sensors.

1. Introduction

Lanthanide materials have excellent luminescence properties such as wide spectral range, long lifetime and sharp bands, which can be widely used in sensors [1], bio-imaging [2], solar cells [3], and many other fields [4–7]. Many lanthanide materials are solubility in organic solvents and can be doped in polymer to fabricate lanthanide doped materials, which have the advantages of low-defect, transparent and anisotropy. Two or more lanthanide complexes doped in a polymer matrix is a highly attractive approach to form the luminescent materials with unique properties. Yang et al. designed lanthanide-doped core-shell nanoparticles for achieving the multicolor-tunable dual-mode emissions under the excitation of 254 nm and 980 nm [8]. Song et al. prepared lanthanide doped polymers with networks for selectively monitoring Zn^{2+} by the ratiometric fluorescence of lanthanide [9]. Among many lanthanide ions, Tb and Eu ions are the typical lanthanide element for Forster resonance energy transfer (FRET) and have the potentially applications [10,11]. Xia et al. designed the lanthanide metal-organic frameworks used for the thermometers [12]. Gu et al. realized a near white-light metal-organic gel material by adjusting the ratio of Tb/Eu and using organic ligand emission [13]. However, further precise regulation of the luminescence for the lanthanide ions co-doped materials is needed.

As known, the luminescence can be modulated by plasmonic nanoparticles due to the local surface plasmon resonance (LSPR) effect. The interactions between light waves and luminescent materials can be unprecedented control by designing and tuning the concentration, size and shape of the plasmonic nanoparticles [14–17]. And the coupling of plasmonic nanostructures

#512053 https://doi.org/10.1364/BOE.512053
Journal © 2024 Received 10 Nov 2023; revised 11 Dec 2023; accepted 12 Dec 2023; published 18 Dec 2023

recently have attracted considerable attention to further improve the luminescence and to realize the modification of the emission pattern [18]. For lanthanide materials, many researches have reported the excitation enhancement and emission enhancement of lanthanide materials caused by plasmonic nanoparticles [19]. Yuan Gao et Al used the LSPR effect of Al nanolars to achieve upconversion luminescence enhancement of (Er/Yb@Yb/Nd) core−shell NPs, and the results showed that the enhancement could reach 44-fold [20]. Avaro Herrera et al made an Er-doped GeO_2·PbO glass for near-infrared luminosity enhancement with an enhancement factor of 1.38-fold using a Au@Ag structure. The mechanism of NIR luminescence enhancement is analyzed in detail [21]. Xiaohu Mi et al. reported a new method for synthesis of Au–Cu Janus nanojellyfish (JNF) by using twinned tips of Au nanoflower (NF) as seeds. The luminescence enhancement of the upconversion nanoparticles is nearly 5000-fold [22]. In addition, experiments have suggested that the energy transfer channel can be turned on/off and modified the energy transfer efficiency in presence of plasmonic nanoparticles [23]. However, most of these systems focused on the maximized enhancement, and it is difficult to realize a uniform luminescence enhancement, which is often beneficial for the practical applications, such as the sensing based on the film platform. There are still rarely plasmonic substrates available to serve as a uniform platform for enhancing the luminescence.

In this work, the Au nanorods (Au NRs) embedded in polyvinyl alcohol (PVA) films are prepared simply and used for the improvement and modulation of the photoluminescence(PL) properties of Tb/Eu films. The emission process of the Tb/Eu films are modulated due to the well match between the transverse LSPR (T-LSPR) and the longitudinal LSPR (L-LSPR) of Au NRs and the emission bands of Tb and Eu respectively. The results shows that the PL of the Tb/Eu film is greatly improved and varied at different zone of the Au NRs-PVA film, the maximum luminescence is obtained near the edge area due to the distribution of Au NRs in PVA film. The luminescence is nearly uniform within a location area of about three times of the incident light spots. Under excitation of 292 nm, the maximum enhancement factor is 37.2-fold for the emission at 612 nm and 21.6-fold for the emission at 545 nm, which can be attributed to the increases of the local density of optical states (LDOS) and the energy transfer efficiency from Tb to Eu. Under excitation of 360 nm, the maximum enhancement factor is 71.5-fold for the emission at 612 nm due to the increase of the LDOS. The dual modulation on the PL and the energy transfer is achieved based on the Au NRs-PVA film.

2. Experiments and methods

2.1. Chemicals and materials

PVA ($(C_2H_4O)_n$,≥99%) was gotten from Kermel. Poly(methylmethacrylate) (PMMA,$(C_5H_8O_2)_n$) was gotten from Acros. For the lanthanide complexes, Tris(2,2,6,6-tetramethyl-3,5-heptanedionato) terbium(III) ($Tb(TMHD)_3$, $C_{27}H_{29}N_2O_6Tb$) was obtained from Aladdin. Tris(1,3-diphenyl-1,3-propanedionato)(1,10-phenanthroline)europium(III) ($Eu(dbm)_3phen$,$C_{57}H_{41}EuN_2O_6$) was obtained from Hwrk Chem. The Si(111) wafer and quartz substrates were bought commercially.

2.2. Preparation of Au NRs-PVA film

The Au NRs were prepared according to our previous method [24]. Detailed experiments were presented in the Part 1 of the Supplement 1. Then, in order to adjust the distribution of the Au NRs on the substrate, the Au NRs solutions were mixed with 2 wt.% PVA solution by volume ratio 1:1 and stirred for 4 h to form Au NRs-PVA solutions. 300 µl of the Au NRs-PVA solution was drop-casted onto the quartz substrate (2 cm×2 cm) and dried in a vacuum oven at 50 °C to get the locally uniform Au NRs-PVA nanocomposite film.

Biomedical Optics EXPRESS

2.3. Preparation of Tb/Eu co-doped PMMA film

The PMMA and rare earth complexes including $Tb(TMHD)_3$ and $Eu(dbm)_3phen$ were dissolved in chloroform, the weight ratio of rare earth complexes, PMMA, and chloroform was 0.03:1:150. The different molar ratios of Tb and Eu were selected, as follows 1:0.0, 1:0.4, 1:0.8, 1:1.0, 1:1.2 and 1:1.4. After the rigorous stirring for 2 h, 60 µl of the prepared solution was taken and spin-coated on substrates with and without Au NRs-PVA film to get the Eu/Tb co-doped film. Then the samples were baked for 30 min. The prepared process of Eu/Tb co-doped film on Au NRs-PVA nanocomposite film is shown in Fig. 1.

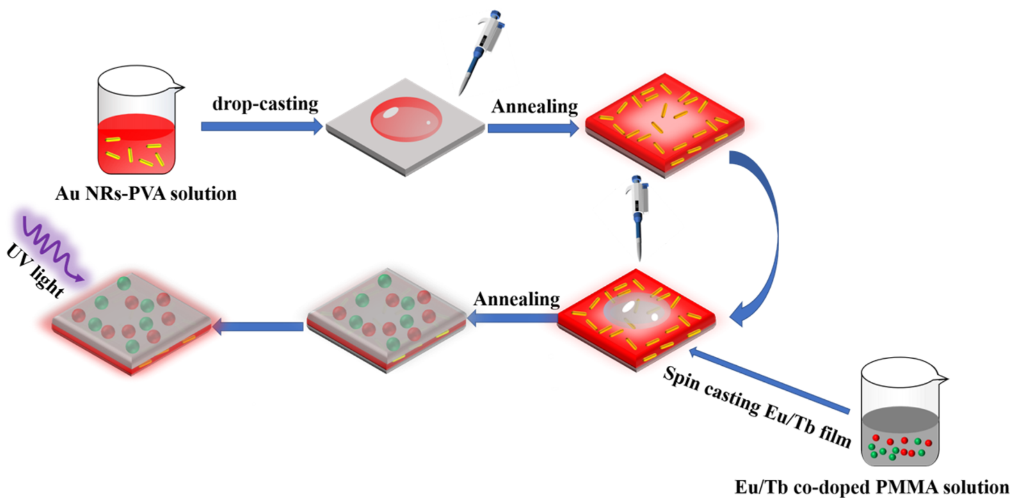

Fig. 1. The prepared process of samples.

2.4. Characterization

The thickness and refractive index of PMMA and PVA films were measured by the Spectroscopic Ellipsometer (J.A.Woollam, M-2000VI). The morphology of Au NRs was measured by transmission electron microscopy (TEM,JEM-2010PLUS) and the distribution was measured by scan electron microscopy (SEM,ZISS sigma 300). The absorption spectra were characterized by the UV-vis spectrometer (HITACHI U-3310). The Fourier Transform Infrared spectra (FT-IR) of samples were collected by the Fourier transform infrared spectroscopy (IRTracer-100). The Microscope photos were obtained by Axio Imager A2 m. The emission spectra were measured by the spectrophotometer system (Edinburgh FLS920), and the luminescence kinetics data was measured by the time-correlated single photon counting technique.

2.5. Theoretical simulations

The electromagnetic field intensity was simulated by the finite difference time domain (FDTD) method. The FDTD simulation was realized by the software of Rsoft. The diameter and length used in simulations were set as about 20 nm and 50 nm respectively according to the experimental data. The Au NR was embedded in a 50 nm PVA film (optimal luminescence enhancement thickness), and Eu or Tb complexes were simulated as dipoles. The dielectric constants of PVA and PMMA films were set as 1.47 and 1.49 respectively. The corresponding grid size was set as 1 nm. A plane-wave total field-scattered field source was used as the incident light.

3. Results and discussion

3.1. Main properties of the Au NRs-PVA nanocomposite films

The properties of the Au NRs-PVA nanocomposite film are investigated, and the results are presented in Fig. 2(a)-(e). The Au NRs in PVA solutions are characterized by TEM, as shown in Fig. 2(a). It is indicated that the Au NRs in the PVA solution is rods, which is the same with that in aqueous solution. The diameter and length distribution of Au NRs are presented in Fig. 2(b)-(c), the corresponding average diameter is about 19.4 ± 2.2 nm and the average length is about 43.5 ± 6.1 nm respectively. The normalized absorption spectra of Au NRs-PVA film (blue line) and Au NRs in aqueous solution (red line) are shown in Fig. 2(d). As shown, there are two plasmon absorption bands located at 518 nm and 633 nm, corresponding the T-LSPR and L-LSPR of the Au NRs in aqueous solution. For the Au NRs-PVA film, the plasmon absorption peaks are red-shifted to 521 nm and 660 nm respectively, the red shift phenomenon can be attributed to the high refractive index of the PVA [25]. The pure PVA film and Au NRs-PVA film are further characterized by FTIR spectra, as shown in Fig. 2(e). For the pure PVA film, a broad absorption band located at 3329 cm^{-1} is observed due to the O-H stretching vibrations. The narrow band located at 2943 cm^{-1} is associated with CH_2-group stretching vibrations. And the peak located at 1095 cm^{-1} corresponds to the C-O stretching and O-H bending vibrations arising from the PVA chain [26]. However, for the Au NRs-PVA film, the vibration bands centered at 3329 cm^{-1}, 2943 cm^{-1}, and 1095 cm^{-1} are sharper than that of the pure PVA film and have the greater intensities due to the existence of Au NRs in PVA film [27].

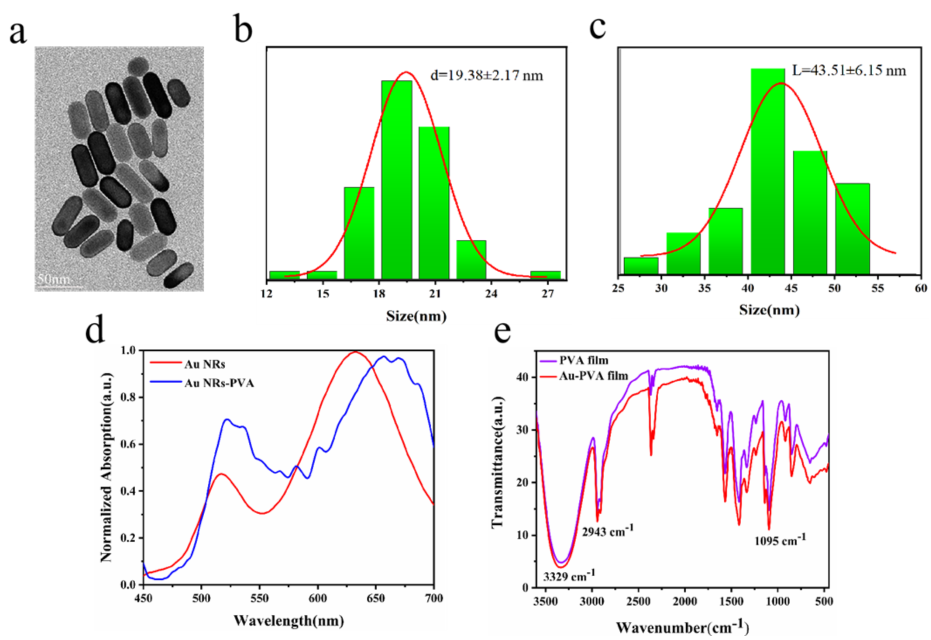

Fig. 2. **a.** TEM image of the Au NRs in PVA solution. **b.** Diameter distribution of Au NRs. **c.** Length distribution of Au NRs. **d.** The absorption of Au NRs-PVA film (blue line) and Au NRs in aqueous solution (red line). **e.** The FTIR spectra of pure PVA film and Au NRs-PVA film.

The entire distribution of plasmonic nanoparticles in PVA film have a great effect on the PL enhancement, which would deduce the different PL enhancement at the different zone for the Eu/Tb film. As known, the distribution can change continuously from a ring to mountainlike when the mobility of the contact line and evaporation rate are changed [28]. For the Au NRs-PVA solution, the distribution of AuNRs would change due to the adhesion of PVA. The comparison of the distribution of the pure Au NRs after drop-casting the pure Au NRs solution and Au NRs-PVA solution under the same conditions are presented, which is shown in Supplementrary Figure S1 and Figure S2. As shown in Figure S1, many coffee-ring pattern can be obtained for the pure Au NRs solution here. Unlike the distribution of the pure Au NRs, there are only a few rings and the ring at the edge is biggest on the substrates for the Au NRs-PVA film, which demonstrates that there are a large number of Au NRs at the edge. Compared with the coffee-ring pattern of the pure Au NRs, the entire distribution of the Au NRs embedded in PVA appears the better dispersion due to the viscosity of PVA. It can realize the uniform distribution of Au NRs within a local range. The EDS images of Au NRs-PVA film near the edge is presented in Supplementary Figure S3, which can further prove the presence of the element Au. Hence, the Au NRs-PVA nanocomposite films can be used as the locally uniform platform for the luminescence enhancement.

To present the effect of the pure PVA and the Au NRs-PVA film on the luminescence, the influence of the pure PVA film and the Au NRs-PVA film on the luminescence of Eu is presented in Figure S4. As shown, the greatest luminescence enhancement based on the pure PVA film is about 2.5-fold and it is obtained at the central zone. And for the Au NRs-PVA film substrates, the greatest luminescence enhancement can reach to dozens of times and the strongest luminescence intensity is obtained at the area of edge due to the distribution of Au NRs as shown in Figure S2d. Moreover, the luminescence intensity of Tb/Eu films based on the Au NRs PVA film at all positions are obviously greater than that based on the pure PVA film. It is further found that the luminescence intensity nearly no change when the measured positions is slightly moved in the local micro-region (about three times the size of the excited light spot), which further prove the uniform distribution of Au NRs within a local range.Hence, the luminescence intensity can be regarded as uniform in the local micro-region due to the distribution of Au NRs here. The locally uniform luminescence enhancement is obtained by the Au NRs-PVA film. According to the results above, all the Tb/Eu co-doped PMMA film on the Au NRs-PVA film is recorded at the edge zone at which the greatest maximum luminescence intensity is obtained in the experiments.

3.2. Luminescence properties of Tb/Eu film based on the Au NRs-PVA nanocomposite films under excitation of 292 nm

The optical properties of Tb film, Eu film and Tb/Eu co-doped PMMA film have been researched in detail before [24]. Here, the pure Tb/Eu co-doped PMMA film has the similar optical properties. Fig. 3 shows the corresponding PL properties of Tb/Eu co-doped PMMA film on the Au NRs-PVA film under excitation of 292 nm. Fig. 3(a) shows the comparison of the luminescence spectra of the Tb/Eu co-doped PMMA film in the presence and absence of Au NRs-PVA film at different molar ratios of Tb and Eu. Inset further shows the luminescence spectra of the Tb/Eu co-doped PMMA film at different molar ratios of Tb and Eu in absence of Au NRs-PVA film. As shown in inset, in absence of Au NRs-PVA film, the luminescence of Tb is decreased and the luminescence of Eu is increased with the increase of the molar ratios of Tb and Eu due to the energy transfer from Tb to Eu. And the PL of Tb/Eu film is extremely improved in presence of Au NRs-PVA film for all the molar ratios. To further present the influence of the Au NRs-PVA film on the PL properties, the corresponding luminescence enhancement factor at 545 nm and 612 nm is shown in Fig. 3(b) respectively. It is shown that the enhancement factor is about 19.3-fold for the pure Tb film. For the Tb/Eu co-doped PMMA film, the enhancement factors at 545 nm and 612 nm both increases to a maximum and then decreases with the increasing of Eu, The enhancement factors at 545 nm are 9.7-fold, 17.6-fold, 21.6-fold, 16.3-fold and 18.5-fold respectively and the enhancement factors at 612 nm are 14.3-fold, 37.2-fold, 32.3-fold, 26.1-fold, and 23.2-fold respectively for the molar ratios of 1: 0.4, 1:0.8, 1:1.0, 1:1.2 and 1:1.4. The maximum enhancement factor is 21.6-fold (545 nm) and 37.2-fold (612 nm) at the molar

Biomedical Optics EXPRESS

ratio of 1:1.0 and 1:0.8 respectively. It can be seen that even under the excitation of 292 nm, the enhancement factor at 612 nm is always higher than that at 545 nm, which can be attributed to the greater relative intensity of L-LSPR than that of T-LSPR.

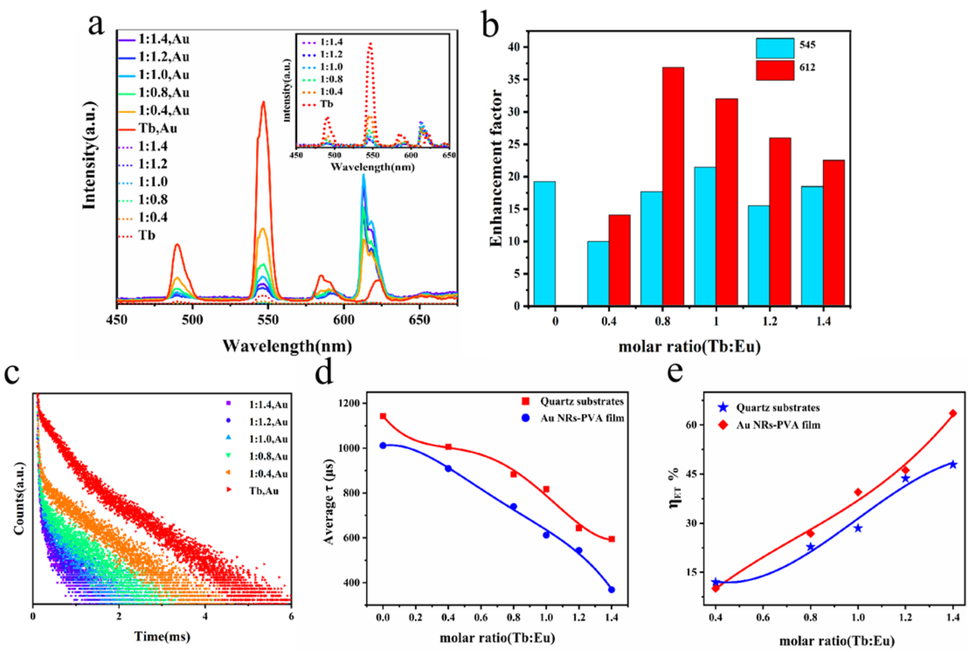

Fig. 3. The PL properties of Tb/Eu co-doped PMMA film on substrates with Au NRs-PVA film under excitation of 292 nm: **a.** The PL spectra with and without Au NRs-PVA film. Inset shows the PL spectra without Au NRs-PVA film. **b.** The corresponding enhancement factors at 545 nm and 612 nm respectively. **c.** The luminescence decay lifetime curves at 545 nm. **d.** The average lifetime of Tb/Eu co-doped film. **e.** The molar ratio dependencies of the efficiency of the energy transfer from the Tb to the Eu.

To further reveal the interaction between Au NRs-PVA film and Tb/Eu film, the change of lifetime for the samples with Au NRs-PVA film are researched. Fig. 3(c) shows the decay curves of the Tb/Eu co-doped PMMA film at 545 nm. Fig. 3(d) shows the corresponding average lifetime at different molar ratios. As shown, the average lifetime is decreased at all the different molar ratios, which is accompanied by a significant increase in luminescence intensity. For pure Tb film, the average lifetime is decreased from 1143.42 μs to 1011.55 μs. For the Tb/Eu co-doped PMMA film, the average lifetime is decreased from 909.39 μs to 368.82 μs with increasing of Eu. All the results reveals the greatly influence of Au NRs-PVA film on the emission process.

As known, the energy transfer from donor to acceptor is an non-radiative process, which would lead to the decrease of the lifetime. The energy transfer efficiencies can be calculated according to the equation $\eta_{ET} = 1 - \frac{\tau}{\tau_0}$, where τ and τ_0 are the luminescence lifetime of the donor in the presence and absence of the acceptor respectively [29]. For the energy transfer from Tb to Eu, the decrease of the lifetime reveal the efficiently energy transfer from Tb to Eu. The decreased lifetime of Tb with the increasing of Eu demonstrates the improvement of the energy transfer efficiency from Tb to Eu. The calculated energy transfer efficiency η_{ET} for the samples with and without Au NRs-PVA film are presented in Fig. 3(e). As shown, for the pure Tb/Eu film in absence of Au NRs-PVA film, the η_{ET} is increased from 12.01% to 47.89% with increasing of Eu. And it is increased from 10.10% to 63.54% in presence of Au NRs-PVA film. The maximum

Biomedical Optics EXPRESS

η_{ET} is increased from 47.89% to 63.54%. It is indicated the energy transfer from Tb to Eu due to the Au NRs-PVA film is increased.

As known, the energy transfer efficiency η_{ET} also can be expressed as:

$$\eta_{ET} = \frac{R_0^6}{R_0^6 + \gamma^6} \tag{1}$$

where R_0 is the Forster distance, γ is the distance between Eu and Tb. In this work, the film is the same, so the distance γ can be set as the same. R_0 is related to the the relative orientation of Eu and Tb transfer dipoles, the refractive index, the fluorescence quantum yield of Tb without Eu, and the overlap of the emission of donor and the absorption of the acceptor [30]. In presence of Au NRs-PVA film, the refractive index measured by ellipsometer is slightly increased, the fluorescence quantum yield and the spectra overlap is also increased, which would deduced the increase of R_0 and the energy transfer efficiency. Hence, the energy efficiency η_{ET} is increased here.

The Au NRs-PVA nanocomposite film used here has two LSPR bands located at 521 nm and 660 nm, which match well with the main emission bands of Tb and Eu respectively. So, the Au NRs embedded in PVA film would mainly modulate the emission process of Tb and Eu due to the Purcell effect [31]. According to Fermi's golden rule, the radiative rate of an emitter can be expressed as follows:

$$K = \frac{\pi\omega}{3\hbar\mathcal{E}_0}|p|^2\rho(r, \omega) \tag{2}$$

where ω is the emission frequency, p is the transition dipole moment of the emitter, r is the position, ε_0 is the permittivity of free space, and $\rho(r, \omega)$ is the LDOS at frequency ω. It can be found that the radiative rate is proportional to the LDOS. When the LSPR of plasmonic nanostructures overlaps well with the emission band of emitters, the LDOS can be obviously improved and further enhances the radiative rate K. According to lifetime $\tau = \frac{1}{K+K_n}$, where K is the radiative rate and K_n is the nonradiative rate. The decreased lifetime accompanied by a significant increase in luminescence intensity here reveals the increase of the radiative rate due to the increased LDOS of emitters [32]. On the other hand, the LDOS at the emitter position has a great relationship with the electromagnetic field enhancement and the transition dipole moment of the emitter [33]. In our experiments, the transition dipole moment of emitters can be set as random in the films. Hence the electromagnetic field enhancement at the emission wavelength provides the insights into the decreased lifetime and the improved LDOS for these samples. The findings above indicate that the Au NRs-PVA film speeds up the emission process of the Tb/Eu co-doped PMMA film at 545 nm, the corresponding radiative rates could be increased by manipulating the LDOS of emitter through the Purcell effect.

Since the LDOS is associated with the electromagnetic field enhancement, the distribution of the local electric field near the Au NRs embedded in 50 nm PVA film is simulated at the excitation and emission wavelengths of the Tb/Eu film by using FDTD method. The parameters in the simulations are selected according to the experimental data. The results are presented in Fig. 4. The red line shown in Fig. 4 represents the interface between Au NRs-PVA film and Tb/Eu co-doped PMMA film. The local electromagnetic field enhancement is firstly presented at different wavelengths. As shown in Fig. 4(a)-(b), the local electric field at 292 nm and 360 nm is slightly enhanced because the overlap between the LSPR bands and the excitation bands located at 292 nm and 360 nm is not well. Figure 4(c)-(d) shows the local field at 545 nm and 612 nm. As shown, the local electric field is remarkably enhanced in the proximity of the Au NRs due to the well overlapping, which reveals the excitation of the LSPR at 545 nm and 612 nm. The maximum intensity of local electric field is observed at 612 nm due to the greater relative intensity of L-LSPR than the T-LSPR, providing insights into the greater enhancement factor at 612 nm for the Tb/Eu co-doped PMMA film.

Biomedical Optics EXPRESS

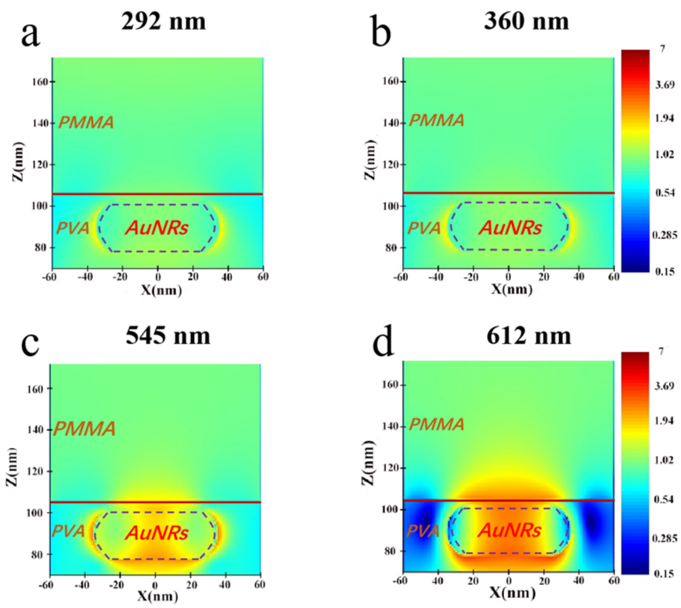

Fig. 4. The simulated distribution of the local electric field based on the Au nanorod embedded in PVA layer at **a.** 292 nm, **b.** 360 nm, **c.** 545 nm, and **d.** 612 nm.

To further present the influence of Au NRs-PVA film on the luminescence process, dipole is further utilized to simulate the Tb or Eu luminescent molecule in the PMMA film based on the Au nanorod embedded in 50 nm PVA. The emission wavelengths of the dipole are set as 545 nm and 612 nm, respectively. The emission of pure dipole in local field zone is shown in Fig. 5(a). And the emission of dipole at 545 nm and 612 nm based on Au NRs-PVA film are shown in Fig. 5(b)-(c) respectively. It is can be seen that the emission at 612 nm is greater along the propagation direction compared with that at 545 nm in local field zone, which is consistent with the experimentally result. To further present it, the intensity of filed along the white dotted line which near the Au NR is shown in Fig. 5(d). As shown, when the dipole is deposited near the Au NR, the emission of dipole is enhanced at 545 nm and 612 nm, and the enhancement at 612 nm is greater than that at 545 nm. The electromagnetic field enhancements at 545 nm and 612 nm reflect that the Au NRs can greatly increase the LDOS and modulate the emission process of Tb and Eu.

Based on above analyses, Fig. 6 indicates the schematic of the PL of Tb/Eu co-doped PMMA film in presence of Au NRs-PVA film. Under excitation of 292 nm, the organic ligand TMHD absorbs the energy and is excited to the excited state S1, and the energy at the excited state S1 is transferred to the triplet excited state of the ligand through inter-system crossing, then transfer the energy to the Tb ions $^5D_4$ level, which induced the excitation of Tb ions [34]. The excited ions Tb partly radiate the energy by the luminescence to emit the green light at 545 nm ($^5D_4 \rightarrow ^7F_5$), and partly transfer the energy to the Eu ions $^5D_0$ level to emit red light at 612 nm ($^5D_0 \rightarrow 7F_2$), which is the energy transfer process between Tb and Eu. According to Purcell effect, the T-LSPR and L-LSPR bands of the Au NRs-PVA film match well with the emission bands of Tb and Eu respectively, which results in the increase of LDOS and the modulation on the emission process of Tb and Eu [19]. The FDTD simulations at the emission wavelength further prove the increase of LDOS due to the Au NRs-PVA film. Meanwhile, the energy transfer from Tb to Eu is also modulated due to the well match. As known, the plasmonic nanostructures nearly the randomly distributed donor-acceptor pairs can effectively influence the FRET, and the energy transfer rate,

Biomedical Optics EXPRESS

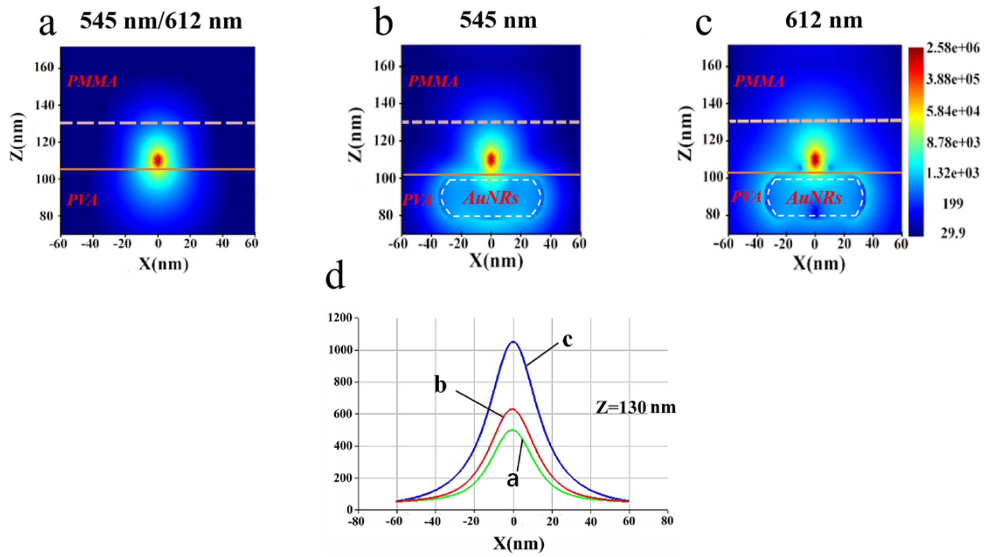

Fig. 5. **a.** the emission of the pure dipole in nearfield range. **b.** the emission of dipole at 545 nm based on Au nanorod embedded in PVA layer. **c.** the emission of dipole at 612 nm based on Au nanorod embedded in PVA layer. d. The field intensity along the white dotted line (z = 130 nm) shown in figure a-c.

efficiency and forster distance can be modified because of the coupling of the fluorophores with Au NRs. When the plasmon peak overlaps with the emission peak of the donor, the energy transfer channel is turned off. When the plasmon is right at the intrinsic emission peak of the acceptor, the energy transfer channel is turned on [35]. Here, the L-LSPR is overlap with the emission of the acceptor and it's stronger than that of the T-LSPR, which results in the increase of the energy transfer efficiency.

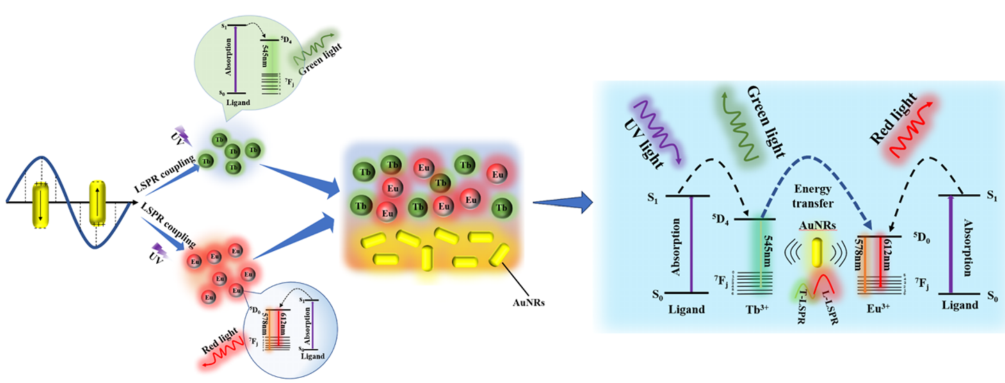

Fig. 6. Schematic of the luminescence of Tb/Eu film in presence of Au NRs-PVA film under excitation of 292 nm.

3.3. *Luminescence properties of Tb/Eu co-doped PMMA film based on the Au NRs-PVA nanocomposite films under excitation of 360 nm*

Under excitation of 360 nm, the emission properties of the Tb/Eu co-doped PMMA film in presence of Au NRs-PVA films are shown in Fig. 7. As shown, the PL at 612 nm is the main emission, the

Biomedical Optics EXPRESS

PL at 545 nm is not obvious because the Tb is not excited at 360 nm. Figure 7(a) shows the PL spectra of the Tb/Eu co-doped PMMA film with and without Au NRs-PVA film respectively. As shown, the PL of samples with Au NRs-PVA film is extremely improved compared with that of the pure Tb/Eu co-doped PMMA film. Figure 7(b) presents the corresponding enhancement factor at 612 nm. The enhancement factor increases to a maximum and then decreases with increasing of Eu. The maximum enhancement factor is up to 71.5-fold at the molar ratio of 1:1, the enhancement factors are 29.2-fold, 56.7-fold, 71.5-fold, 65.5-fold and 55.5-fold respectively with the increase of the molar ratios, which is extremely greater than that under the excitation of 292 nm (Fig. 3(b)). The comparison of the enhancement factor under excitation of 292 nm and 360 nm is shown in Supplementary Figure S5. Under excitation of 292 nm, although the samples are excited under the characteristic excitation of Tb, the enhancement factor at the emission of 612 nm is greater than that at the emission of 545 nm. The greater enhancement factor at 612 nm is because that the relative intensity of L-LSPR is greater than that of the T-LSPR as shown in Fig. 2(d), which means the greater influence on the radiative rate at 612 nm. Under excitation of 292 nm, the Au NRs can be used for the increase of the LDOS and modulate the emission of Eu and Tb at 612 nm and 545 nm respectively, meanwhile the energy transfer between Tb and Eu is also increased. For emission of 612 nm, the enhancement factor under excitation of 360 nm is greater than that under excitation of 292 nm. Under excitation of 360 nm, the Au NRs only can be used for modulate the luminescence of Eu at 612 nm because the emission at 545 nm is not excited then, which would result in the greater increase of the LDOS and deduce the greater enhancement factor at 612 nm.

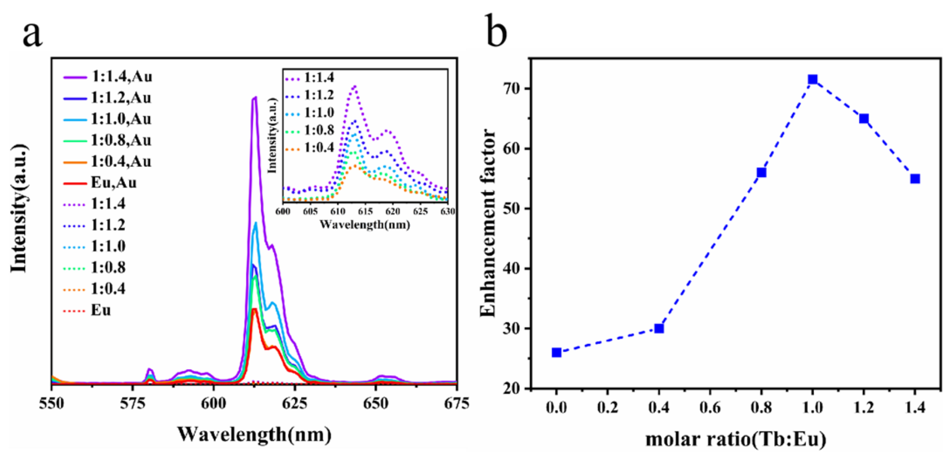

Fig. 7. The emission properties of samples: **a.** The photoluminescence spectra of the Tb/Eu co-doped PMMA film without and with Au NRs-PVA film under excitation of 360 nm. Inset is the corresponding luminescence spectra without Au NRs-PVA film under excitation of 360 nm. **b.** The corresponding enhancement factor.

Many investigates have realized the regulation of the luminescence properties of rare earth co-doped materials by the plasmonic nanoparticles. For example, Xin Li et al. designed recyclable upconversion fluorescence indicator papers consisting of upconversion nanorods and plasmonic nanostructures by electrospinning to achieve $NaYF_4$:Yb^{3+},Er^{3+} 3-fold enhancement [6]. Yuan Zhao et al prepared Au nanobipyramids (Au NBPs) and persistent luminescence ZnGeGaO:Cr,Er,Yb nanoparticle (ZGGO NP) nanocomposites to enhance the luminescence of materials with an enhancement factor of 1.5-fold [36]. Zongzhuo Xie et al propose a technological approach to combine core - shell structures and plasmon resonance for synergistically enhancing the luminescence intensity with tunable upconversion luminescence emission. The results show

Biomedical Optics EXPRESS

that the overall upconversion luminescence is improved by two orders of magnitude [37]. For our sample, the Tb/Eu luminescence are enhanced by tens of times due to the introduction of Au NRs. At the same time, the energy transfer from Tb to Eu is improved, resulting in a change in the red-green intensity ratio. More importantly, the locally uniform luminescence enhancement is obtained, which has the potential for application in the field of fluorescence detection. In addition, the LSPR effect of metal nanoparticles has also been applied to optical fiber sensors. For example, Ragini Singh et al. prepared a novel tape-in-taper with four tapered (TIT4 T) structure based on single-mode fiber. The functionalized Au NPs particles were further immobilized in the probe's sensing region to increase its LSPR efficiency and sensitivity. The low concentration and repeatable detection of ALT is realized by the change of the absorption peak of Au NPs [38]. And it has been reported that the PVA film has the good biocompatible [39]. Therefore, the Au NRs-PVA film here may also be coated on the surface of the fiber and used as the potential optical fiber sensors.

Conclusion

The Au NRs-PVA films are prepared easily and used as a platform to achieve the locally uniform luminescence enhancement, the luminescence of Tb/Eu co-doped PMMA films is obviously enhanced. Under excitation of 292 nm, the maximum enhancement factors are 37.2-fold at 612 nm and 21.6-fold at 545 nm, respectively. This can be attributed to the improved LDOS and increased energy transfer efficiency between Tb and Eu as a result of the Au NRs-PVA film. Under excitation of 360 nm, the maximum enhancement factor is approximately 71.5-fold for the emission at 612 nm. In this case, the Au NRs-PVA film is used to modulate the emission process at 612 nm, which induced a greater enhancement factor. This study of Au NRs-PVA film on the luminescence properties of co-doped films has great application potential and can be used as a useful platform for several applications, such as thin film-based detectors and sensors. The platform would demonstrate the excellent detection performance and enhance the sensitivity through the luminescence enhancement of the Tb/Eu films. Its locally uniform luminescence can make it to be a valuable tool in fluorescence detection and realize the enhanced sensitivity of detection. And it is also a candidate material in the field of optical fiber sensors. By adjusting the plasmonic nanoparticles and choosing the rare earth ions, it can be used to detect a wide range of substances.

Funding. Natural Science Foundation of Shandong Province (ZR2019MF068, ZR2022MF240); Science and Technology Plan of Youth Innovation Team for Universities of Shandong Province (2019KJJ019).

Disclosures. The authors declare no conflicts of interest.

Data availability. Data underlying the results presented in this paper are not publicly available at this time but may be obtained from the authors upon reasonable request.

Supplemental document. See Supplement 1 for supporting content.

References

1. Y. Zhao, X. Wang, Y. Zhang, *et al.*, "Optical temperature sensing of up-conversion luminescent materials: Fundamentals and progress," J. Alloys Compd. **817**, 152691 (2020).
2. Q. Fan, X. Cui, H. Guo, *et al.*, "Application of rare earth-doped nanoparticles in biological imaging and tumor treatment," J. Biomater. Appl. **35**(2), 237–263 (2020).
3. F. Zhao, Y. Liang, J. B. Lee, *et al.*, "Applications of rare earth Tb^{3+}-Yb^{3+} co-doped down-conversion materials for solar cells," Mater. Sci. Eng., B **248**, 114404 (2019).
4. Y. Hua and J. S. Yu, "Dual-functional platforms toward field emission displays and novel anti-counterfeiting strategy based on rare-earth activated materials," Ceram. Int. **47**(13), 18003–18011 (2021).
5. J. Zhang, X. Li, J.-C. Zhang, *et al.*, "Ultrasensitive and reusable upconversion-luminescence nanofibrous indicator paper for in-situ dual detection of single droplet," Chem. Eng. J. **382**, 122779 (2020).
6. X. Li, J. Zhang, J. C. Zhang, *et al.*, "Ultrasensitive and Recyclable Upconversion-Fluorescence Fibrous Indicator Paper with Plasmonic Nanostructures for Single Droplet Detection," Adv. Opt. Mater. **7**(19), 1900364 (2019).
7. J. Zhang, S. Li, D.-D. Ju, *et al.*, "Flexible inorganic core-shell nanofibers endowed with tunable multicolor upconversion fluorescence for simultaneous monitoring dual drug delivery," Chem. Eng. J. **349**, 554–561 (2018).

8. M. Ding, B. Dong, Y. Lu, *et al.*, "Energy Manipulation in Lanthanide-Doped Core-Shell Nanoparticles for Tunable Dual-Mode Luminescence toward Advanced Anti-Counterfeiting," Adv. Mater. (Weinheim, Ger.) **32**(45), 2002121 (2020).
9. X.-Q. Song, H.-H. Meng, Z.-G. Lin, *et al.*, "2D Lanthanide Coordination Polymers: Synthesis, Structure, Luminescent Properties, and Ratiometric Sensing Application in the Hydrostable PMMA-Doped Hybrid Films," ACS Appl. Polym. Mater. **2**(4), 1644–1655 (2020).
10. Y. Sohn, "Contour mapping 2D and 3D-photoluminescence of Au-doped one-dimensional Eu(III) and Tb(III) hydroxide and oxide nanostructures," Ceram. Int. **39**(8), 9157–9161 (2013).
11. L. Liu, M. Yu, J. Zhang, *et al.*, "Facile fabrication of color-tunable and white light emitting nano-composite films based on layered rare-earth hydroxides," J. Mater. Chem. C **3**(10), 2326–2333 (2015).
12. T. Xia, Z. Shao, X. Yan, *et al.*, "Tailoring the triplet level of isomorphic Eu/Tb mixed MOFs for sensitive temperature sensing," Chem. Commun. **57**(25), 3143–3146 (2021).
13. D. Gu, W. Yang, D. Lin, *et al.*, "Water-stable lanthanide-based metal–organic gel for the detection of organic amines and white-light emission," J. Mater. Chem. C **8**(39), 13648–13654 (2020).
14. H. Wei, X. Yan, and Y. Niu, "Plasmon–exciton interactions: Spontaneous emission and strong coupling," Adv. Funct. Mater. **31**(51), 2100889 (2021).
15. Z. Zuo, L. Sun, Y. Guo, *et al.*, "Multiple plasmon couplings in 3D hybrid Au-nanoparticles-decorated Ag nanocone arrays boosting highly sensitive surface enhanced Raman scattering," Nano Res. **15**(1), 317–325 (2022).
16. C. Folks, U. S. Phuyal, M. Rajesh, *et al.*, "Fabrication and comparative quantitative analysis of plasmonic-polymer nanocomposites as optical platforms," Langmuir **37**(44), 12853–12866 (2021).
17. O. Pavelka, S. Dyakov, J. Vesely, *et al.*, "Optimizing plasmon enhanced luminescence in silicon nanocrystals by gold nanorods," Nanoscale **13**(9), 5045–5057 (2021).
18. J. Zhang, X. Cheng, H. Zhang, *et al.*, "Plasmon-Controlled Selective Emission Enhancement of Eu^{3+} with (AuCore)@(Y(V,P)O4:Eu) Nanostructures," ACS Nano **17**(11), 10546–10559 (2023).
19. X. Qin, A. Carneiro Neto, R. Longo, *et al.*, "Surface plasmon–photon coupling in lanthanide-doped nanoparticles," J. Phys. Chem. Lett. **12**(5), 1520–1541 (2021).
20. Y. Gao, S. Murai, K. Shinozaki, *et al.*, "Up-conversion Luminescence Enhanced by the Plasmonic Lattice Reso nating at the Transparent Window of Water," ACS Appl. Energy Mater. **4**(4), 2999–3007 (2021).
21. A. Herrera, O. Restrepo, and N. Balzaretti, "Formation of Au@Ag Bimetallic Nanoparticles via Ion Implantation and Its Effects on Boosting the Near-Infrared Emission of Er^{3+} Ions in Germanate Glass for Applications in Optical Amplifiers," J. Phys. Chem. C **127**(1), 133–141 (2023).
22. X. Mi, X. Zhao, and M. Ji, "Twinned-Au-tip-induced growth of plasmonic Au–Cu Janus nanojellyfish in upconvers ion luminescence enhancement," J. Colloid Interface Sci. **624**, 196–203 (2022).
23. S. Hou, Y. Chen, D. Lu, *et al.*, "A self-assembled plasmonic substrate for enhanced fluorescence resonance energy transfer," Adv. Mater. (Weinheim, Ger.) **32**(8), 1906475 (2020).
24. Q. Wang, J. Liu, K. Huang, *et al.*, "Dual coupled effects of low concentration gold nanorods on energy transfer and luminescence enhancement in Eu/Tb co-doped films," Spectrochim. Acta, Part A **235**, 118260 (2020).
25. A. Hu, W. Zhang, S. Liu, *et al.*, "In situ scattering of single gold nanorod coupling with monolayer transition metal dichalcogenides," Nanoscale. **11**(43), 20734–20740 (2019).
26. U. Lad, G. M. Kale, and R. Bryaskova, "Glucose oxidase encapsulated polyvinyl alcohol-silica hybrid films for an electrochemical glucose sensing electrode," Anal. Chem. **85**(13), 6349–6355 (2013).
27. A. Gautam, P. Komal, R. Sevak Singh, *et al.*, "Hard core proof of the polyvinyl alcohol as a reducer for the formation of gold nanoparticles," J. Lumin. **334**, 116112 (2021).
28. X. Man and M. Doi, "Ring to mountain transition in deposition pattern of drying droplets," Phys. Rev. Lett. **116**(6), 066101 (2016).
29. S. Gopi, S. K. Jose, E. Sreeja, *et al.*, "Tunable green to red emission via Tb sensitized energy transfer in Tb/Eu codoped alkali fluoroborate glass," J. Lumi. **192**, 1288–1294 (2017).
30. H. Y. Liu, C. Y. Li, J. Li, *et al.*, "Plasmon-enhanced fluorescence resonance energy transfer in different nanostructures and nanomaterials,," Appl. Mater. Today **30**, 101731 (2023).
31. J. Liu, X. Zhao, X. Liu, *et al.*, "Enhanced luminescence of Eu-doped films based on gap coupled plasmons," J. Alloys Compd. **907**, 164451 (2022).
32. H. Kishida and M. H. Mikkelsen, "Ultrafast lifetime and bright emission from graphene quantum dots using plasmonic nanogap cavities," Nano Lett. **22**(3), 904–910 (2022).
33. J. Feng and H. Zhang, "Hybrid materials based on lanthanide organic complexes: a review," Chem. Soc. Rev. **42**(1), 387–410 (2013).
34. R. Ishimatsu, E. Kunisawa, K. Nakano, *et al.*, "Electrogenerated Chemiluminescence and Electronic States of Several Organometallic Eu(III) and Tb(III) Complexes: Effects of the Ligands," Chem. Select. **4**, 2815–2831 (2019).
35. L. Zhao, T. Ming, L. Shao, *et al.*, "Plasmon-controlled forster resonance energy transfer[J]," J. Phys. Chem. C **116**(14), 8287–8296 (2012).
36. Y. Zhao, L. Shi, and H. Miao, ""Add on" dual-modal optical immunoassay by plasmonic metal NP-semiconductor composites," Anal. Chem. **93**(6), 3250–3257 (2021).
37. Z. Xie, Z. Shu, N. Tu, *et al.*, "Rationally-designed core–shell structure with double-plas mon effect for efficient and tunable upconversion luminescence emission," Appl. Surf. Sci. **643**, 158726 (2024).

Biomedical Optics EXPRESS

38. R. Singh, Z. Wang, and C. Marques, "Alanine aminotransferase detection using TIT assisted four tapered fiber structure-based LSPR sensor: From healthcare to marine life," Biosens. Bioelectron. **236**, 115424 (2023).
39. B. Zhang, Z. Jiang, and X. Li, "Facile preparation of biocompatible and antibacterial water-soluble films using polyvinyl alcohol/carboxymethyl chitosan blend fibers via centrifugal spinning," Carbohydr. Polym. **317**, 121062 (2023).